



## Early View

### Original research article

## **Intracellular hydroxyproline imprinting following resolution of bleomycin-induced pulmonary fibrosis**

Shengren Song, Zhenli Fu, Ruijuan Guan, Jie Zhao, Penghui Yang, Yang Li, Hang Yin, Yunxin Lai, Gencheng Gong, Simin Zhao, Jiangtian Yu, Xiaomin Peng, Ying He, Yumei Luo, Nanshan Zhong, Jin Su

Please cite this article as: Song S, Fu Z, Guan R, *et al.* Intracellular hydroxyproline imprinting following resolution of bleomycin-induced pulmonary fibrosis. *Eur Respir J* 2021; in press (<https://doi.org/10.1183/13993003.00864-2021>).

This manuscript has recently been accepted for publication in the *European Respiratory Journal*. It is published here in its accepted form prior to copyediting and typesetting by our production team. After these production processes are complete and the authors have approved the resulting proofs, the article will move to the latest issue of the ERJ online.

## **Intracellular Hydroxyproline Imprinting Following Resolution of Bleomycin-Induced Pulmonary Fibrosis**

Shengren Song<sup>1, 2, 5#</sup>, Zhenli Fu<sup>2#</sup>, Ruijuan Guan<sup>3#</sup>, Jie Zhao<sup>4#</sup>, Penghui Yang<sup>2#</sup>, Yang Li<sup>4</sup>, Hang Yin<sup>2</sup>, Yunxin Lai<sup>2</sup>, Gencheng Gong<sup>2</sup>, Simin Zhao<sup>2</sup>, Jiangtian Yu<sup>3</sup>, Xiaomin Peng<sup>2</sup>, Ying He<sup>2</sup>, Yumei Luo<sup>2</sup>, Nanshan Zhong<sup>1, 2\*</sup>, Jin Su<sup>2, 3\*</sup>

### **Affiliations:**

<sup>1</sup>Department of Pathophysiology, Guizhou Medical University, Guiyang, Guizhou, China;

<sup>2</sup>State Key Laboratory of Respiratory Diseases, National Clinical Research Center for Respiratory Diseases, Guangzhou Institute of Respiratory Health, the First Affiliated Hospital of Guangzhou Medical University, Guangzhou, Guangdong, China;

<sup>3</sup>Shenzhen International Institute for Biomedical Research, Shenzhen, Guangdong, China;

<sup>4</sup>Guangdong Provincial Key Laboratory of Biomedical Imaging and Guangdong Provincial Engineering Research Center of Molecular Imaging, The Fifth Affiliated Hospital, Sun Yat-sen University, Zhuhai, China;

<sup>5</sup>Affiliated Hospital of Guizhou Medical University, Guiyang, Guizhou, China.

### **\*Correspondence:**

Dr. Jin Su, State Key Lab of Respiratory Diseases, National Clinical Research Center for Respiratory Disease, Guangzhou Institute of Respiratory Health, The First Affiliated Hospital, Guangzhou Medical University, Guangzhou, China. Email: [sujin@gird.cn](mailto:sujin@gird.cn).

Or Dr. Nanshan Zhong, Department of Pathophysiology, Guizhou Medical University, Guiyang, Guizhou, China. Email: [nanshan@vip.163.com](mailto:nanshan@vip.163.com).

<sup>#</sup>These authors contributed equally to this work.

**ABSTRACT** Idiopathic pulmonary fibrosis (IPF) is a fatal lung disease with few treatment options. The poor success in developing anti-IPF strategies have impelled researchers to reconsider the importance of choice for animal model and assessment methodologies. Currently, it is still not settled whether the bleomycin-induced lung fibrosis mouse model finally returns to resolution.

This study aimed to follow the dynamic fibrotic features of BLM (Bleomycin)-treated mouse lungs with extended durations through a combination of the latest technologies (micro-CT imaging and histological detection of degraded collagens) with traditional methods. In addition, we also applied immunohistochemistry to explore the distribution of all hydroxyproline-containing molecules.

As determined by classical biochemical method, total lung hydroxyproline contents reached peak at 4-week after bleomycin injury and maintained a steady high level thereafter until the end of the experiments (16-week). This result seemed to partially contradict with the changes of other fibrosis evaluation parameters, which indicated a gradual degradation of collagens and a recovery of lung aeration post the fibrosis peak. This inconsistency was well reconciled by our data from immunostaining against hydroxyproline and a fluorescent peptide staining against degraded collagen, together showing large amounts of hydroxyproline-rich degraded collagen fragments detained and enriched within the intracellular regions at 10- or 16-week, rather than at 4-week post the BLM-treatment. Hence, our present data not only offer respiratory researchers a new perspective towards the resolution nature of mouse lung fibrosis, but also remind them to be cautious while using hydroxyproline content assay to evaluate the severity of fibrosis.

## **Introduction**

Idiopathic pulmonary fibrosis (IPF), characterized by the distortion of lung architecture and deposition of extracellular matrix (ECM), is a chronic, progressive and usually lethal lung disease of unknown etiology, with a 5-year survival of approximately 20% [1]. IPF affects ~5 million people worldwide, and its incidence increases dramatically with age [2]. According to the calculation data from a most recent review published in *European Respiratory Journal* [3], there were a total of 145 IPF clinical trials that investigated 93 compounds/combinations in the past decade. Disappointingly, these tremendous investments only facilitated the approval of two drugs (pirfenidone and nintedanib). Albeit having shown some benefits in slowing down the pace of lung function decline, these two anti-fibrotic drugs failed to improve the overall survival of IPF patients [4].

Experimental models are indispensable and crucial tools for understanding the pathogenesis of lung diseases as well as for evaluating drug efficacy prior to conducting clinical trials. The poor success in developing anti-IPF strategies has impelled many researchers and experts to reinforce and emphasize the importance of choice for appropriate animal model and reliable assessment methodologies in recent years [3, 5-9]. Intratracheal instillation of bleomycin in mice, albeit its limitations, is still the most frequently used and best accepted lung fibrosis model due to its gross similarities to IPF patients, low cost, relative ease of induction and high reproducibility [6, 9]. There is, at least, one consensus about this model: inflammatory infiltration usually occurs within 7 days, followed by a gradual accumulation of ECM proteins thereafter and a peak fibrotic response at around 3-4 weeks later [3]. However, one point still remaining unsettled disputes is that whether the bleomycin-induced fibrotic lung injury finally returns to normal or partial resolution [9]. Early studies claimed to observe a self-limiting response of fibrosis in mice [10-13], which contrasts with the progressive and irreversible nature of human IPF. On the contrary, there are other reports showing that the bleomycin-induced fibrosis

in C57BL/6J mice can persist up to 3-6 months and the injury in the lung never resolves [14, 15]. The reason for this discrepancy remains unresolved and was speculated to be associated with the dosing of bleomycin and/or murine strains used by different researchers [9].

In considering that the readouts for fibrosis intensity and distribution adopted by previous studies were mostly achieved through sacrificing animals at various time points, it is necessary to combine non-invasive approaches with optimized classical methods so as to reconcile the above debate. Conventional methodologies used for lung fibrosis assessments include biochemical quantification of collagen (hydroxyproline content as a surrogate or Sirius red staining), histologic assessment of fibrotic distribution (Masson's trichrome staining), and gene expression analysis of fibrotic markers. Due to the patchy distribution of bleomycin-induced fibrotic lesions as well as the inherent bias associated with morphological scoring systems, the 2017 guidelines of the American Thoracic Society strongly recommended hydroxyproline measurement of the whole lung homogenates as the optimal primary endpoint for preclinical assessment of potential therapies against pulmonary fibrosis [6]. While gene expression studies were suggested to be used accompanied with biochemical parameters. To decrease the observer-dependent variability of morphological examination and scoring systems, advanced computer machine learning tools were recently developed and utilized to quantitatively analyze the fibrotic areas on the whole-slide images (WSI) of lung tissues from either animal models or human patients [16, 17].

Computed tomography (CT), a non-invasive imaging technique that provides accurate longitudinal information, now plays a central role in the diagnosis of IPF via recognition of usual interstitial pneumonia (UIP) patterns characterized by reticulation and honeycomb cysts of subpleural and bibasilar distribution [18]. Because this clinically relevant method complies with "the 3R rules" (Refinement, Replacement, Reduction) in animal experimentation, the micro-CT machine correspondingly was vastly applied to small rodent pulmonary fibrosis models [15, 19-21]. Representative two-dimensional micro-CT images of the lung were initially used to depict the

severity of lung injury in animals. Due to the patchy and heterogeneous nature of the bleomycin-induced model, later it became a tendency to perform three-dimensional reconstruction of the lung CT images in order to measure the residual lung volumes according to the corresponding range of Hounsfield Unit (HU) value [22-24], a quantitative radiodensity scale. Notably, by selecting pixels with a HU ranging from -121~121, the lung CT images of bleomycin mouse model were subtly segmented into four zones with different aeration status, including normal aeration, poor aeration, hyperinflation as well as non-aeration [23].

Here we aimed to dynamically follow the fibrotic features of bleomycin-treated mouse lungs with extended durations (up to 16 weeks) through a combination of the above latest technologies with traditional methods. The results showed that, at later stages of fibrosis, alterations in hydroxyproline content that is long considered as a “golden standard” for lung fibrosis assessment did not coincide with the changes of other evaluation parameters, including histologic staining, gene expression as well as lung aeration. This striking exceptional result was confirmed to be associated with the incomplete removal of degraded collagen fragments, as demonstrated by immunostaining of hydroxyproline. Hence, the data from the current study offer all respiratory researchers a new perspective towards the resolution nature of mouse lung fibrosis.

## **Methods**

For detailed methods including animal protocols and experimental procedures, see the supplementary material.

### *Ethics statement*

All animal experiments were approved by the Animal Care and Use Committee of Guangzhou Medical University, and were performed in strict accordance with approved guidelines.

### *Statistics*

Data were processed with the GraphPad Prism software (version 6.0; San Diego, CA, USA), and are expressed as the mean  $\pm$  SEM. One-way analysis of variance (ANOVA) with Bonferroni post-hoc test was used to compare differences among various groups. A value of  $p < 0.05$  was considered statistically significant.

### **Results**

#### *Biochemical determination of collagen content.*

In order to dynamically characterize the fibrosis patterns in bleomycin-treated lungs, the mice receiving a single intratracheal instillation of bleomycin were sacrificed at various intervals for up to 16 weeks after injury (**figure 1a**). The whole lung tissue homogenates were firstly subjected to a colorimetric-based hydroxyproline assay, a method for collagen content determination with most high-priority recommendations [6, 25, 26]. The results showed that the total lung hydroxyproline contents were inclined to gradually increase from week 1 to week 4 and maintained unchanged thereafter (**figure 1b**). Because some of the above observed phenomena were apparently contradictory with the data reported elsewhere showing that the bleomycin-induced lung hydroxyproline content usually dropped to the basal level from 8-week onwards [12, 27, 28], another batch of mice was utilized to repeat this study. It was demonstrated that from week 4 to week 16, mouse hydroxyproline levels remained steadily high (**Online supplementary figure. Sa**), implying that the data from our model system were highly repeatable and confirmed.

To further test whether the lung hydroxyproline contents in bleomycin-induced mouse model were in proportion to their corresponding amounts of native collagens, Sirius red staining that allows analysis of “newly formed” collagen fibers was then performed on the same animals. Unlike the alteration patterns in hydroxyproline, collagen fibers displayed a dramatic increase at the initial 4 weeks but significantly trended downwards at 16-week follow-ups (**figure 1c and 1d**). These results indicate that the fibrotic lung microenvironment in mice might shift from collagen synthesis to degradation following week 4.

*Gene expression analysis of extracellular matrix (ECM) molecules.*

Gene expression analysis of major components of extracellular matrix (ECM) represents another assessment option for the severity of lung fibrosis [6]. As demonstrated by the results of real-time quantitative PCR (qPCR) and western blot (**figure 2a-c and online supplementary figure. Sb**), the mRNA and protein expressions of both fibronectin and collagen- I were markedly elevated to peak values at around week 2 to 3, and then followed by a reduction to the basal level at week 16, suggesting that the deposited ECM induced by bleomycin in mice might have reached to a peak prior to week 4.

*Quantification of the extent of lung damage as well as the collagen structure on histological image.*

Nextly, the structural changes of the bleomycin-treated lung were histopathologically examined by H&E staining. To minimize observer-dependent biases, the stained lung tissue sections were scanned by a commercial WSI scanner to obtain high-resolution digital images of the entire sections and then subjected to quantitative calculation of damaged areas by use of a novel automated tool called Orbit Image Analysis [16]. Consistent to the above collagen expression data, the proportions of injured regions exhibited a significant augment from week 1 to 4 and then appeared to decrease from week 10 to 16 (**figure 3a and 3b**).

The hallmark structure of collagen is the triple helix where three linear protein chains assemble into a trimetric form. Upon fragmented by proteases such as the MMPs, the collagen molecule denatures as the triple helix unfolds [29]. The collagen hybridization peptide (CHP) is a synthetic peptide that can specifically bind to such degraded and denatured collagen molecules, but not the intact collagen [29]. Using fluorescently labeled CHP (Cy5-CHP), we tested whether the molecular structure of collagen in the lung tissue is intact at week 16. There were minimal fluorescent CHP signals in the interstitial areas in the normal lung, and the signal gradually increases from week 1 to week 4 of fibrosis (**figure 4a and 4b**). The fluorescence intensity

peaked at week 16 in the lung, at a level that was significantly higher than week 4. These data strongly support the conception that the collagen matrix did undergo a degradative process from week-4 toward week-16.

#### *In vivo micro-CT analysis of lung structure and aeration*

To further validate the above *in-vitro* tissue data as well as to reduce animal-to-animal variability, the *in vivo* changes in lung structure or function were dynamically monitored by micro-CT imaging which can provide longitudinal information on the same individual animal [6]. Representative lung transverse micro-CT sections from week 1 to week 16 post-bleomycin were shown in **figure 5**. It was demonstrated that the areas of lung consolidation reached maximum level at week 4 and then gradually dwindled, hinting a recovery course at later stages of fibrosis.

To more subtly segment out those lung regions with partial or complete loss of aeration, a novel algorithm established by a most recent study was also introduced into the present study, which accomplished in the discrimination of poorly-aerated and non-aerated regions with the HU thresholds ranging from -434 to -121 HU and -120 to 121 HU, respectively [23]. As indicated by **figure 6a**, the three types of regions with different conditions of aeration in fibrotic mice matched well with the visible structural alterations on transverse CT sections, suggesting the reliability of this method. Further lung volumetric analysis showed that the proportions of both poorly-aerated and non-aerated regions were significantly increased before week 4 and then pronouncedly decreased between week 10 to 16, whereas, those of normally-aerated areas exhibited opposite trend (**figure 6b**). This result can be additionally validated by statistically measuring the corresponding values of multiple animals (**figure 6c**). Collectively, this part of *in vivo* data imply that the bleomycin-triggered lung fibrosis was apt to spontaneously resolve.

#### *Immunohistochemical assay of hydroxyproline-containing molecules.*

Because the hydroxyproline biochemical assay in tissues was conducted on their completely hydrolyzed products, this method in theory can

detect all forms of hydroxyproline-containing substance within tissues. Thus, we infer that the unchanged content of hydroxyproline under conditions of collagen degradation might be resulted from their incomplete removal from the tissue. To confirm this hypothesis, mouse lung tissues were subjected to immunohistochemical staining with specific antibody against hydroxyproline so as to observe its localization. The lung interstitium in control mice were nearly negative for hydroxyproline, whereas, those areas in the group of week-4 exhibited a wide distribution and moderate increase of hydroxyproline accumulation. In sharp contrast, at 10- or 16-week, the positive areas for hydroxyproline, albeit displaying a much more contractible scope, had dramatically enhanced intensity, as compared to those at week 4 (**figure 7a**). Notably, there occurred a crowd of cells with extremely strong intracellular immunostaining of hydroxyproline at both 10- and 16-week (**figure 7a, arrow**). While hydroxyproline-positive molecules appeared to be predominantly located within extracellular regions at 4-week time point. The total intensities of immunostaining signals for hydroxyproline were calculated to have no significant difference between week 4 and week 16 (**figure 7b**), which perfectly agrees with the data from biochemical method. This first application of hydroxyproline-specific immunohistochemistry in lung fibrosis evaluation clearly indicated that hydroxyproline-rich collagen fragments could not be completely removed and catabolized even after long-term evolution of fibrosis (**figure 8**).

## **Discussion**

To our knowledge, this represents the most thorough and deep description of bleomycin-induced pulmonary fibrosis process to date. In addition to traditional methods, several latest improved technologies for fibrosis assessment were also deliberately introduced and utilized, such as AI analysis of whole-slide images, CT-based quantification of lung aeration as well as determination of the unique triple helical structure of collagen by CHP staining. Except for biochemical assay of hydroxyproline content, most of the data from this study agree well with the popular conception that mouse lung fibrosis can spontaneously resolve. This odd

inconsistency was finally reconciled by our application of immunohistochemistry to detect the distribution of hydroxyproline-containing molecules within fibrotic lung tissues.

Here three different aspects of evidences were presented to address a shift in the balance from collagen synthesis to degradation during the whole process of experimental fibrosis. Firstly, the expression of type I collagen, at the level of both transcription and translation, was dramatically decreased after a transient rise during the first 4 weeks. Secondly, Sirius red staining, considered to be specifically suitable for the evaluation of very small fibrotic lesions due to high sensitivity [30], further confirmed the latter decline in new collagen proteins. Thirdly, CHP staining of unfolded collagen chains directly validated the advent of collagen degradation post fibrosis peak. However, our biochemical determination of hydroxyproline obtained contradictory data, showing that the amount of total lung hydroxyproline reached peak at 4-week after bleomycin injury and maintained a steady high level thereafter until the end of the experiments (16-week). The exceptional hydroxyproline data prompts us to firstly reconsider the potential influence from methodologies. Hydroxyproline can be quantified by HPLC, whereas, the most widely used method is a colorimetric assay based on the reaction of oxidized hydroxyproline with *p*-dimethylaminobenzaldehyde [31]. By carefully searching the published literature for detailed information regarding hydroxyproline content in mouse lung fibrosis model, we found two articles had reported similar results with ours, with one using HPLC [15], and the other one utilizing colorimetric assay [14]. Because these two previous independent studies did not investigate the exact status of native collagens, it remains unclear whether the non-equivalence of hydroxyproline content with native collagen quantity in the present study could be similarly observed. While whatever the conclusion is, at least the phenomenon that the bleomycin-induced augmentation of lung hydroxyproline in mice can sustain for a long duration has been demonstrated elsewhere [14, 15].

Collagen degradation occurs through both extracellular and intracellular pathways. The extracellular pathway involves cleavage of collagen fibrils by proteolytic enzymes. While, the intracellular pathway involves binding and uptake of collagen fragments by fibroblasts or macrophages for lysosomal degradation [32]. In theory, biochemical determination of hydroxyproline is supposed to detect all forms of hydroxyproline-containing substance, including native collagens, collagen fragments and free hydroxyproline. Therefore, elevated lung hydroxyproline content after injury, in addition to representing an increase in collagen production, can also mean a defect in complete turnover of collagens [33]. Several pathways have been identified to internalize collagen fragments and consequently allow the cells to clear and recycle matrix components [33-35]. Interestingly, compared with controls, mice deficient in those receptors responsible for collagen internalization exhibit increased total lung hydroxyproline content 4 weeks after bleomycin injury without alterations in inflammation or rates of collagen synthesis [33, 35]. Nevertheless, herein we did not find any significant changes in the expression levels of these genes between group of week-4 and week-16 (data not shown), implying that the process of collagen internalization might function properly during this period. This speculation can be strengthened by the fact that hydroxyproline-rich molecules mostly reside within intracellular compartments of the cell at 10- or 16-week, a phenomenon which is completely absent at 4-week. According to these evidences, the maintenance of extraordinary high level of hydroxyproline at the resolution phase of lung fibrosis might be highly caused by the incomplete clearance of collagen degradation products from the intracellular space (**figure 8**). Future studies need to focus on clarifying the detailed mechanisms underlying collagen turnover during the time window of lung fibrosis resolution.

In mammalian cells, there are a variety types of protein modification at post-translational level, such as phosphorylation, ubiquitination as well as hydroxylation. These modified amino groups can be immunoblotted with corresponding antibodies in combination with immunoprecipitation manipulation. As for anti-hydroxyproline antibody, it was mostly exploited to detect the events of

proline hydroxylation of intracellular signal transducers [36, 37]. While in the fields of organ fibrosis, biochemical assay of hydroxyproline has long been used as the golden standard for collagen content evaluation. Therefore, the current study represents the first to introduce immunoassay of hydroxyproline to fibrosis study.

Even our data and explanation seem reasonable, one point that could not be neglected is that the hydroxyproline content in those studies claiming the resolving nature of bleomycin model trended downwards post the fibrosis peak [28, 38, 39], which is totally opposed to our current data. Although it remains unclear whether this discrepancy is associated with the source of bleomycin or animal species, we at least provide a possibility that the deposited collagens in mouse lung fibrosis model might have the chance to be incompletely cleared under some circumstance. In addition, we also provide a powerful and easy-to-use technique to explore the destination of collagen degradation products in fibrotic lung tissues. This is propitious to reconcile the debate regarding the fibrosis recovery issue that is currently highly dependent on biochemical assay of hydroxyproline.

Although CT scan can report the dynamic structural alterations caused by fibrotic lesions and thus provide longitudinal and localization information, lung CT imaging of small animals has been remaining a challenge due to its relatively low resolution. CT can be calibrated using a reference value of the air (-1,000 HU), pure water (0 HU) and dense bone (+1000 HU). Two recent studies have tried to use the HU value to subdivide the ventilated areas of fibrotic lesions in mice. Although Francesca *et al.* defined poorly-aerated areas in a range of -500 to -100 HU [40], they did not distinguish non-aerated regions which usually have a HU value higher than -100 HU. On the ground of analyzing a large number of lung CT images of pulmonary fibrosis mice, another study proposed a new stratification standard for lung ventilation, which classified the poorly-aerated and non-aerated regions as -434 to -121 HU and -120 to 121 HU, respectively [23]. We applied this novel algorithm to the current study and found that the lung ventilation function tended to spontaneously recover since 4-week after bleomycin, backing the self-limiting nature of this murine model reported by others [12, 28, 41]. To the best of our knowledge, this is the first paper to calculate the

3D volume of lung lesions with different aeration conditions during sustained progression of experimental lung fibrosis and will definitely act as a more reliable functional read-out for future drug efficacy evaluation.

Regarding the multiple methodologies for fibrosis quantitation, we still believe that biochemical assay of hydroxyproline contents is the most objective and accurate one if collagen matrix synthesis dominates over destruction. However, in some cases, such as when studying long duration of fibrosis or evaluating the efficacy of therapeutic agents that are potentially involved in collagen degradation, immunohistochemistry of hydroxyproline as well as CHP staining of denatured collagen are recommended in the first place to confirm whether intensive collagen degradation takes place. In summary, the data from the current study not only offers respiratory researchers a new perspective towards the resolution nature of mouse pulmonary fibrosis process, but also reminds them to be cautious while using conventional hydroxyproline assay to reflect the amounts of collagens.

**Author contributions:** JS, NSZ conceived the project and designed experiments. JS and RJG wrote the manuscript. PHY, YL and YXL edited the manuscript. SRS, ZLF, JZ, HY and GCG performed experiments. SRS, ZLF, JZ, YH, and YML conducted data analysis. All authors have read and approved the final manuscript.

**Support statement:** This work was supported by grants from the National Natural Science Foundation of China (31671472, 81800072), the China Postdoctoral Science Foundation (2020T130027ZX), Guangdong Key Research and Development Project 2020B1111330001 and the COVID-19 Emerging Prevention Products, Research Special Fund of Zhuhai City (ZH22036302200024PWC).

**Conflict of interest:** None declared.

## References:

1. Martinez FJ, Collard HR, Pardo A, Raghu G, Richeldi L, Selman M, Swigris JJ, Taniguchi H, Wells AU. Idiopathic pulmonary fibrosis. *Nat Rev Dis Primers* 2017; 3:17074.
2. Raghu G. Epidemiology, survival, incidence and prevalence of idiopathic pulmonary fibrosis in the USA and Canada. *Eur Respir J* 2017; 49.
3. Kolb P, Upagupta C, Vierhout M, Ayaub E, Bellaye PS, Gauldie J, Shimbori C, Inman M, Ask K, Kolb MRJ. The importance of interventional timing in the bleomycin model of pulmonary fibrosis. *Eur Respir J* 2020; 55.
4. Cruwys S, Hein P, Humphries B, Black D. Drug discovery and development in idiopathic pulmonary fibrosis: challenges and opportunities. *Drug Discov Today* 2020; 25:2277-2283.
5. Spagnolo P, Maher TM. Clinical trial research in focus: why do so many clinical trials fail in IPF? *Lancet Respir Med* 2017; 5:372-374.
6. Jenkins RG, Moore BB, Chambers RC, Eickelberg O, Konigshoff M, Kolb M, Laurent GJ, Nanthakumar CB, Olman MA, Pardo A, Selman M, Sheppard D, Sime PJ, Tager AM, Tatler AL, Thannickal VJ, White ES, Cell ATSAoR, Molecular B. An Official American Thoracic Society Workshop Report: Use of Animal Models for the Preclinical Assessment of Potential Therapies for Pulmonary Fibrosis. *Am J Respir Cell Mol Biol* 2017; 56:667-679.
7. Tashiro J, Rubio GA, Limper AH, Williams K, Elliot SJ, Ninou I, Aidinis V, Tzouveleakis A, Glassberg MK. Exploring Animal Models That Resemble Idiopathic Pulmonary Fibrosis. *Front Med (Lausanne)* 2017; 4:118.
8. Bonniaud P, Fabre A, Frossard N, Guignabert C, Inman M, Kuebler WM, Maes T, Shi W, Stampfli M, Uhlig S, White E, Witzernath M, Bellaye PS, Crestani B, Eickelberg O, Fehrenbach H, Guenther A, Jenkins G, Joos G, Magnan A, Maitre B, Maus UA, Reinhold P, Vernooij JHJ, Richeldi L, Kolb M. Optimising experimental research in respiratory diseases: an ERS statement. *Eur Respir J* 2018; 51.
9. Liu T, De Los Santos FG, Phan SH. The Bleomycin Model of Pulmonary Fibrosis. *Methods Mol Biol* 2017; 1627:27-42.
10. Moore BB, Hogaboam CM. Murine models of pulmonary fibrosis. *Am J Physiol Lung Cell Mol Physiol* 2008; 294:L152-60.
11. Borzone G, Moreno R, Urrea R, Meneses M, Oyarzun M, Lisboa C. Bleomycin-induced chronic lung damage does not resemble human idiopathic pulmonary fibrosis. *Am J Respir Crit Care Med* 2001; 163:1648-53.
12. Lawson WE, Polosukhin VV, Stathopoulos GT, Zoia O, Han W, Lane KB, Li B, Donnelly EF, Holburn GE, Lewis KG, Collins RD, Hull WM, Glasser SW, Whitsett JA, Blackwell TS. Increased and prolonged pulmonary fibrosis in surfactant protein C-deficient mice following intratracheal bleomycin. *Am J Pathol* 2005; 167:1267-77.
13. Chung MP, Monick MM, Hamzeh NY, Butler NS, Powers LS, Hunninghake GW. Role of repeated lung injury and genetic background in bleomycin-induced fibrosis. *Am J Respir Cell Mol Biol* 2003; 29:375-80.
14. Limjunyawong N, Mitzner W, Horton MR. A mouse model of chronic idiopathic pulmonary fibrosis. *Physiol Rep* 2014; 2:e00249.
15. Scotton CJ, Hayes B, Alexander R, Datta A, Forty EJ, Mercer PF, Blanchard A, Chambers RC. Ex vivo micro-computed tomography analysis of bleomycin-induced lung fibrosis for preclinical drug evaluation. *Eur Respir J* 2013; 42:1633-45.

16. Stritt M, Stalder AK, Vezzali E. Orbit Image Analysis: An open-source whole slide image analysis tool. *PLoS Comput Biol* 2020; 16:e1007313.
17. Seger S, Stritt M, Vezzali E, Nayler O, Hess P, Groenen PMA, Stalder AK. A fully automated image analysis method to quantify lung fibrosis in the bleomycin-induced rat model. *PLoS One* 2018; 13:e0193057.
18. Cocconcelli E, Balestro E, Biondini D, Barbiero G, Polverosi R, Calabrese F, Pezzuto F, Lacedonia D, Rea F, Schiavon M, Bazzan E, Foschino Barbaro MP, Turato G, Spagnolo P, Cosio MG, Saetta M. High-Resolution Computed Tomography (HRCT) Reflects Disease Progression in Patients with Idiopathic Pulmonary Fibrosis (IPF): Relationship with Lung Pathology. *J Clin Med* 2019; 8.
19. Ruscitti F, Ravanetti F, Essers J, Ridwan Y, Belenkov S, Vos W, Ferreira F, KleinJan A, van Heijningen P, Van Holsbeke C, Cacchioli A, Villetti G, Stellari FF. Longitudinal assessment of bleomycin-induced lung fibrosis by Micro-CT correlates with histological evaluation in mice. *Multidiscip Respir Med* 2017; 12:8.
20. Lee HJ, Goo JM, Kim NR, Kim MA, Chung DH, Son KR, Kim HC, Lee CH, Park CM, Chun EJ, Im JG. Semiquantitative measurement of murine bleomycin-induced lung fibrosis in in vivo and postmortem conditions using microcomputed tomography: correlation with pathologic scores--initial results. *Invest Radiol* 2008; 43:453-60.
21. Ruscitti F, Ravanetti F, Donofrio G, Ridwan Y, van Heijningen P, Essers J, Villetti G, Cacchioli A, Vos W, Stellari FF. A Multimodal Imaging Approach Based on Micro-CT and Fluorescence Molecular Tomography for Longitudinal Assessment of Bleomycin-Induced Lung Fibrosis in Mice. *J Vis Exp* 2018.
22. Zhou Y, Chen H, Ambalavanan N, Liu G, Antony VB, Ding Q, Nath H, Eary JF, Thannickal VJ. Noninvasive imaging of experimental lung fibrosis. *Am J Respir Cell Mol Biol* 2015; 53:8-13.
23. Mecozzi L, Mambrini M, Ruscitti F, Ferrini E, Ciccimarra R, Ravanetti F, Sverzellati N, Silva M, Ruffini L, Belenkov S, Civelli M, Villetti G, Stellari FF. In-vivo lung fibrosis staging in a bleomycin-mouse model: a new micro-CT guided densitometric approach. *Sci Rep* 2020; 10:18735.
24. Bell RD, Rudmann C, Wood RW, Schwarz EM, Rahimi H. Longitudinal micro-CT as an outcome measure of interstitial lung disease in TNF-transgenic mice. *PLoS One* 2018; 13:e0190678.
25. Campa JS, McAnulty RJ, Laurent GJ. Application of high-pressure liquid chromatography to studies of collagen production by isolated cells in culture. *Anal Biochem* 1990; 186:257-63.
26. Kliment CR, Englert JM, Crum LP, Oury TD. A novel method for accurate collagen and biochemical assessment of pulmonary tissue utilizing one animal. *Int J Clin Exp Pathol* 2011; 4:349-55.
27. Gharaee-Kermani M, Hatano K, Nozaki Y, Phan SH. Gender-based differences in bleomycin-induced pulmonary fibrosis. *Am J Pathol* 2005; 166:1593-606.
28. Caporarello N, Meridew JA, Jones DL, Tan Q, Haak AJ, Choi KM, Manlove LJ, Prakash YS, Tschumperlin DJ, Ligresti G. PGC1alpha repression in IPF fibroblasts drives a pathologic metabolic, secretory and fibrogenic state. *Thorax* 2019; 74:749-760.

29. Hwang J, Huang Y, Burwell TJ, Peterson NC, Connor J, Weiss SJ, Yu SM, Li Y. In Situ Imaging of Tissue Remodeling with Collagen Hybridizing Peptides. *ACS Nano* 2017; 11:9825-9835.
30. Malkusch W, Rehn B, Bruch J. Advantages of Sirius Red staining for quantitative morphometric collagen measurements in lungs. *Exp Lung Res* 1995; 21:67-77.
31. Hofman K, Hall B, Cleaver H, Marshall S. High-throughput quantification of hydroxyproline for determination of collagen. *Anal Biochem* 2011; 417:289-91.
32. McKleroy W, Lee TH, Atabai K. Always cleave up your mess: targeting collagen degradation to treat tissue fibrosis. *Am J Physiol Lung Cell Mol Physiol* 2013; 304:L709-21.
33. Atabai K, Jame S, Azhar N, Kuo A, Lam M, McKleroy W, Dehart G, Rahman S, Xia DD, Melton AC, Wolters P, Emson CL, Turner SM, Werb Z, Sheppard D. Mfge8 diminishes the severity of tissue fibrosis in mice by binding and targeting collagen for uptake by macrophages. *J Clin Invest* 2009; 119:3713-22.
34. Lee W, Sodek J, McCulloch CA. Role of integrins in regulation of collagen phagocytosis by human fibroblasts. *J Cell Physiol* 1996; 168:695-704.
35. Bundesmann MM, Wagner TE, Chow YH, Altemeier WA, Steinbach T, Schnapp LM. Role of urokinase plasminogen activator receptor-associated protein in mouse lung. *Am J Respir Cell Mol Biol* 2012; 46:233-9.
36. Arquier N, Vigne P, Duplan E, Hsu T, Therond PP, Frelin C, D'Angelo G. Analysis of the hypoxia-sensing pathway in *Drosophila melanogaster*. *Biochem J* 2006; 393:471-80.
37. Luo W, Hu H, Chang R, Zhong J, Knabel M, O'Meally R, Cole RN, Pandey A, Semenza GL. Pyruvate kinase M2 is a PHD3-stimulated coactivator for hypoxia-inducible factor 1. *Cell* 2011; 145:732-44.
38. Hecker L, Logsdon NJ, Kurundkar D, Kurundkar A, Bernard K, Hock T, Meldrum E, Sanders YY, Thannickal VJ. Reversal of persistent fibrosis in aging by targeting Nox4-Nrf2 redox imbalance. *Sci Transl Med* 2014; 6:231ra47.
39. Cabrera S, Selman M, Lonzano-Bolanos A, Konishi K, Richards TJ, Kaminski N, Pardo A. Gene expression profiles reveal molecular mechanisms involved in the progression and resolution of bleomycin-induced lung fibrosis. *Am J Physiol Lung Cell Mol Physiol* 2013; 304:L593-601.
40. Ruscitti F, Ravanetti F, Bertani V, Ragionieri L, Mecozzi L, Sverzellati N, Silva M, Ruffini L, Menozzi V, Civelli M, Villetti G, Stellari FF. Quantification of Lung Fibrosis in IPF-Like Mouse Model and Pharmacological Response to Treatment by Micro-Computed Tomography. *Front Pharmacol* 2020; 11:1117.
41. Glasser SW, Hagood JS, Wong S, Taype CA, Madala SK, Hardie WD. Mechanisms of Lung Fibrosis Resolution. *Am J Pathol* 2016; 186:1066-77.

## Figure legends

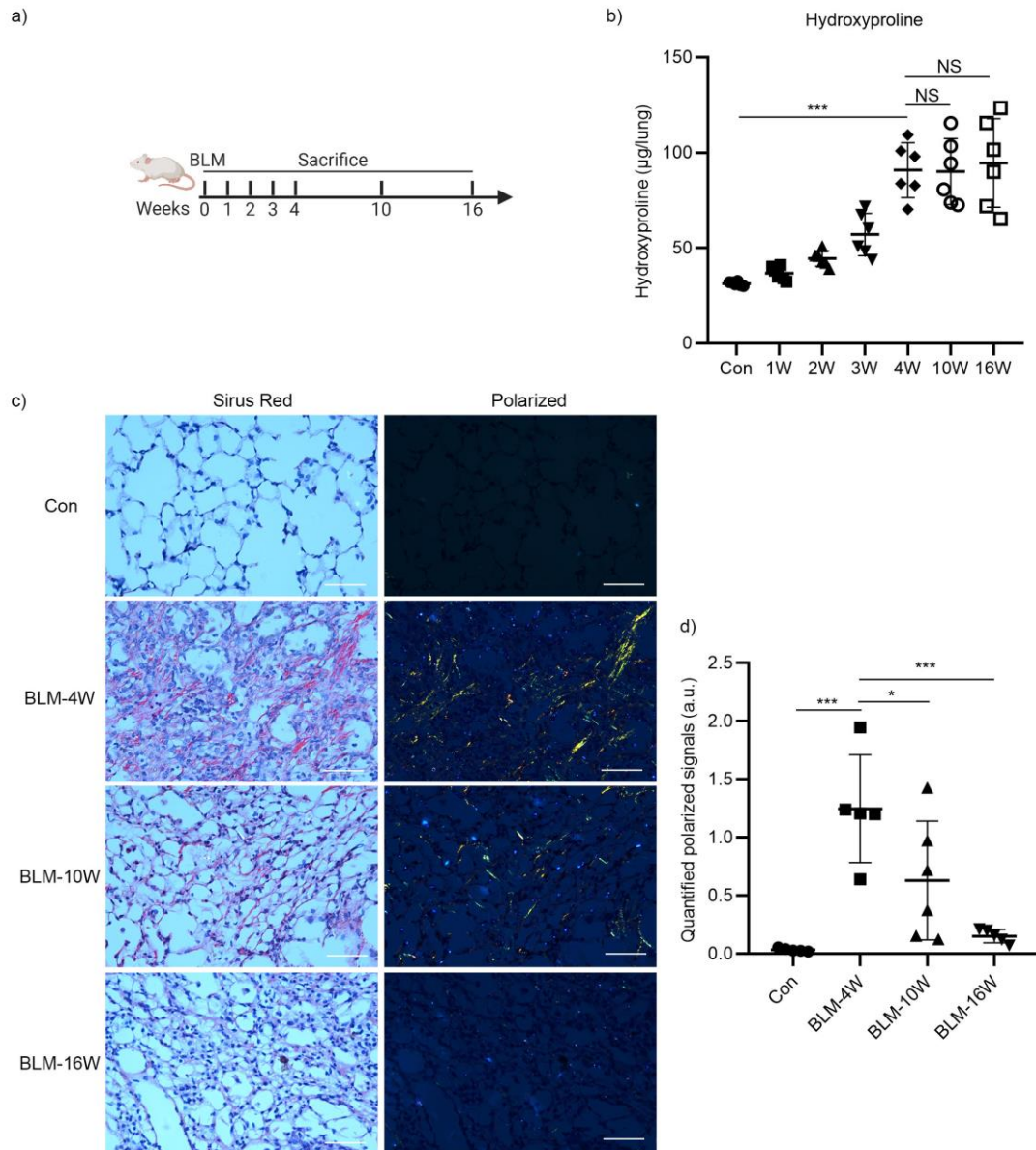


**Figure 1. Lung collagen measurement by biochemical methods during the process of experimental lung fibrosis.** a) The scheme of mice sacrificing following bleomycin instillation. b) A colorimetric-based hydroxyproline assay of bleomycin- or saline-treated mice. c) Sirius red staining of lung tissue sections. The collagen fibers were visualized by polarized light microscopy. Scale bar = 100 µm. d) Quantification of polarized light signals by Image J. Data were expressed as mean ± SD, n = 6, \* p<0.05; \*\*\* p<0.001.

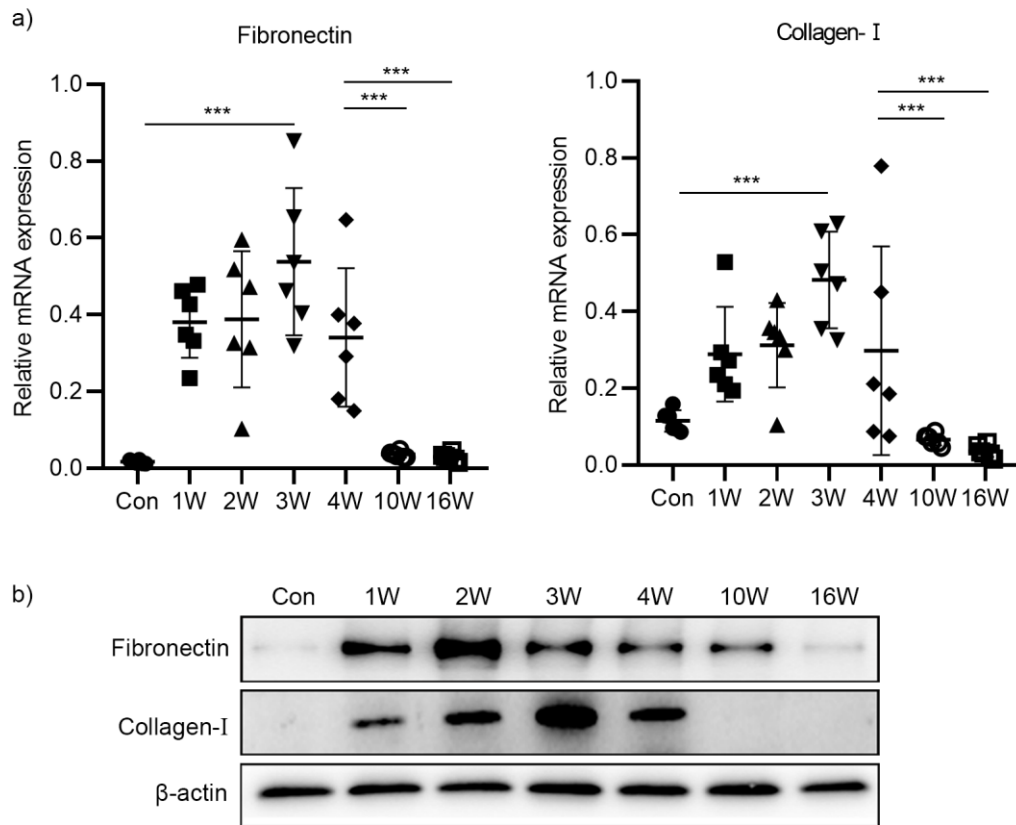


**Figure 2. Gene expression of ECM markers.** The mouse lung tissues at the indicated time points were subjected to either qPCR a) or immunoblot b) analysis of the expression levels of collagen- I and fibronectin, respectively. *Gapdh* and  $\beta$ -actin were used as internal reference controls for qPCR and immunoblot, respectively. qPCR data were expressed as mean  $\pm$  SD, n = 6, \*\*\*p<0.001.

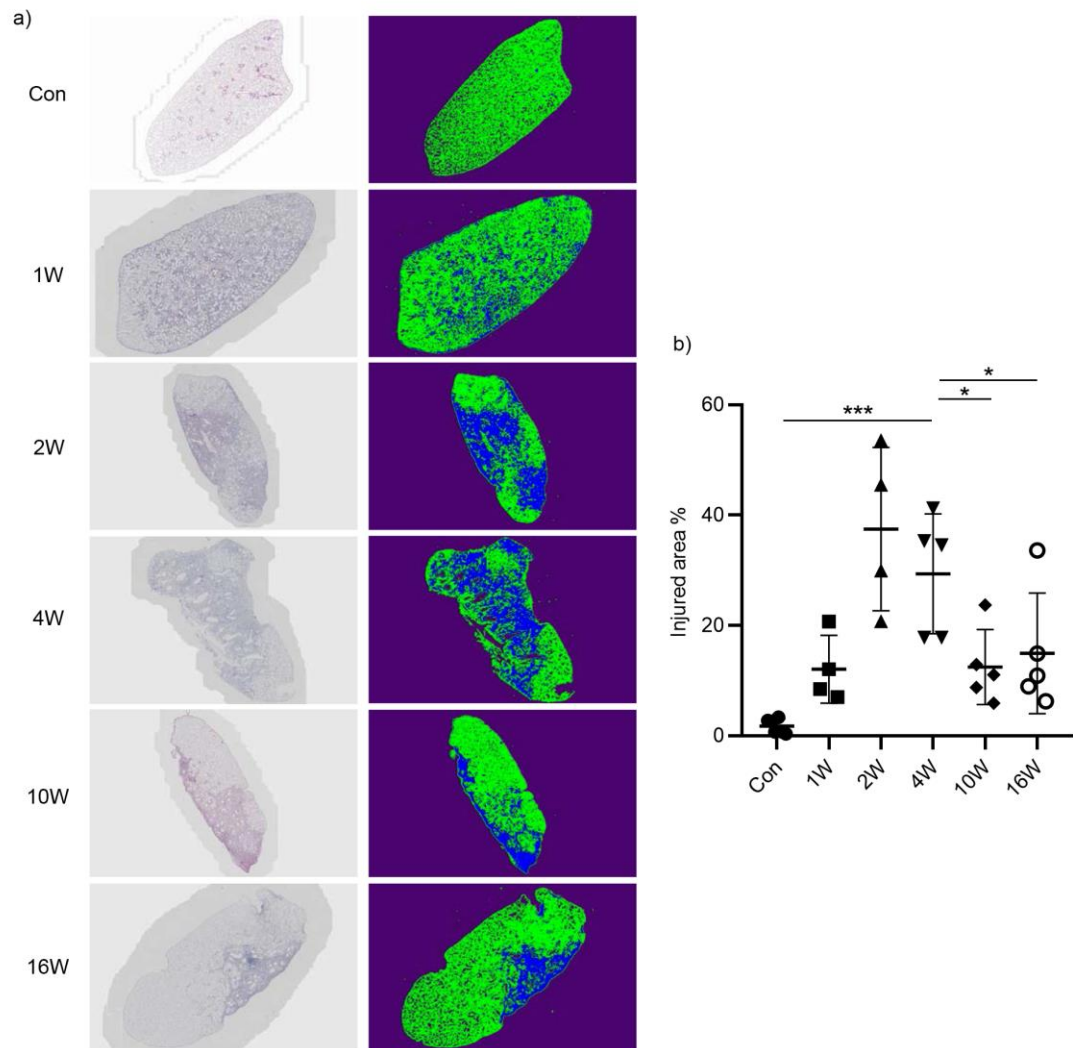


**Figure 3. Histological assessment of lung tissues.** a) Representative H&E-stained WSI images (*left*) and their AI-processed results (*right*) with a software called Orbit Image Analysis. b) Calculation of the percentage of injured areas on H&E WSI images. Data are expressed as mean  $\pm$  SD, n = 4, \* p<0.05; \*\*\* p<0.001.

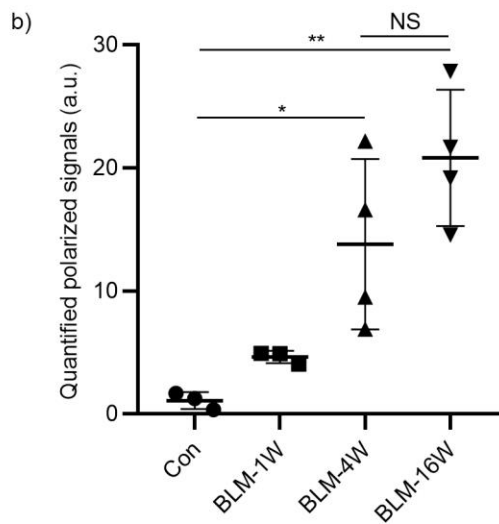
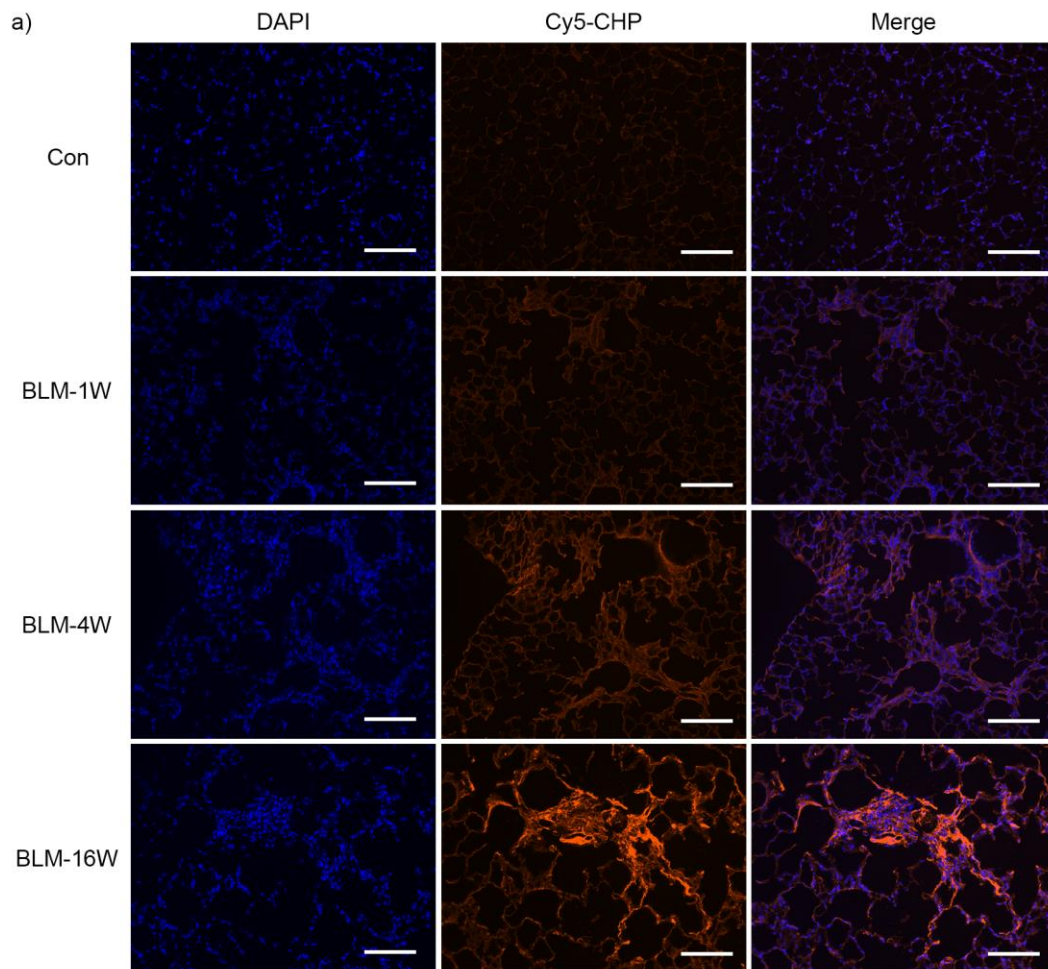


**Figure 4. Histological detection of degraded collagens.** a) Representative fluorescence micrographs of the fibrotic lung areas obtained from mice treated with bleomycin for varying time periods versus control mice treated with saline, and

stained with Cy5-CHP and DAPI. Selected micrographs are representative of images collected from per group. Scale bar=200  $\mu\text{m}$ . b) Quantified polarized signals showing the time course of Cy5-CHP signal levels. Data are expressed as mean  $\pm$  SD, n = 3-6, \*p<0.05, \*\*p<0.01.

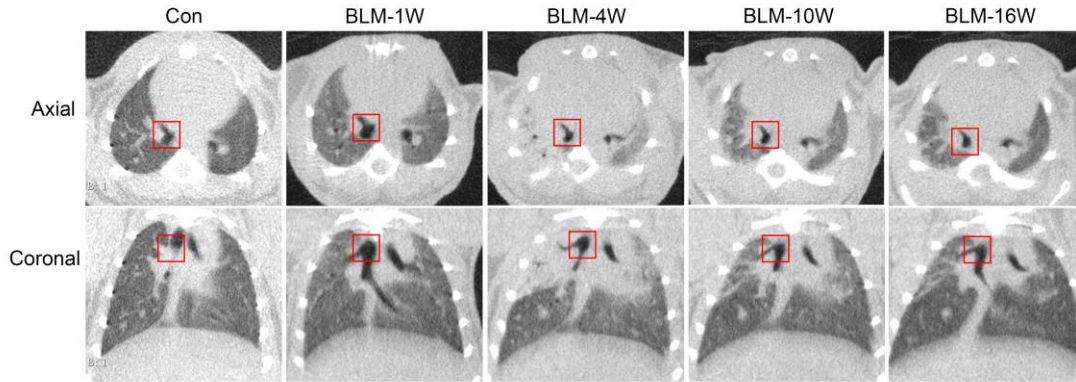


**Figure 5. Micro-CT images of the lungs.** Axial (*top row*) and corresponding coronal (*bottom row*) micro-CT images were acquired at different time points after bleomycin administration at the dose of 2.0 mg/kg. At each time point, the bifurcation of the right bronchus in mice was marked with red square in order to ensure that a region was selected at the same position in all the CT images.

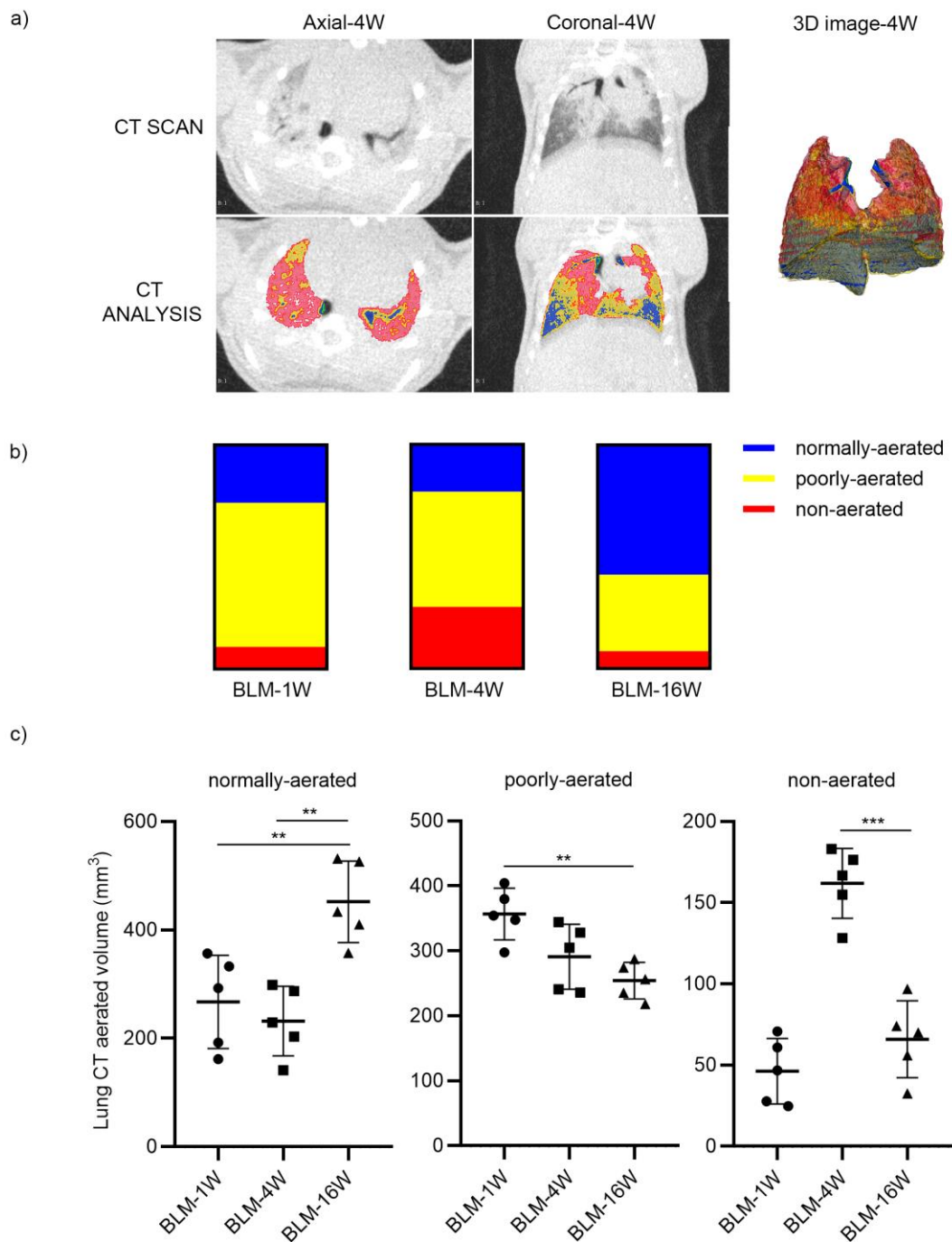


**Figure 6. Quantitative CT volumetric evaluation of lung aeration.** a) Representative colormap of lung CT images of bleomycin-treated mice at week-4. Blue: normally-aerated region; Yellow: poorly-aerated region; Red: non-aerated region. b) Dynamic percentages of lung CT aerated volume in representative mouse at the indicated time points post bleomycin injury. c) Statistical calculation of lung CT aerated volume. Data are expressed as mean  $\pm$  SD, n = 6, \*\* p<0.01; \*\*\* p<0.001.

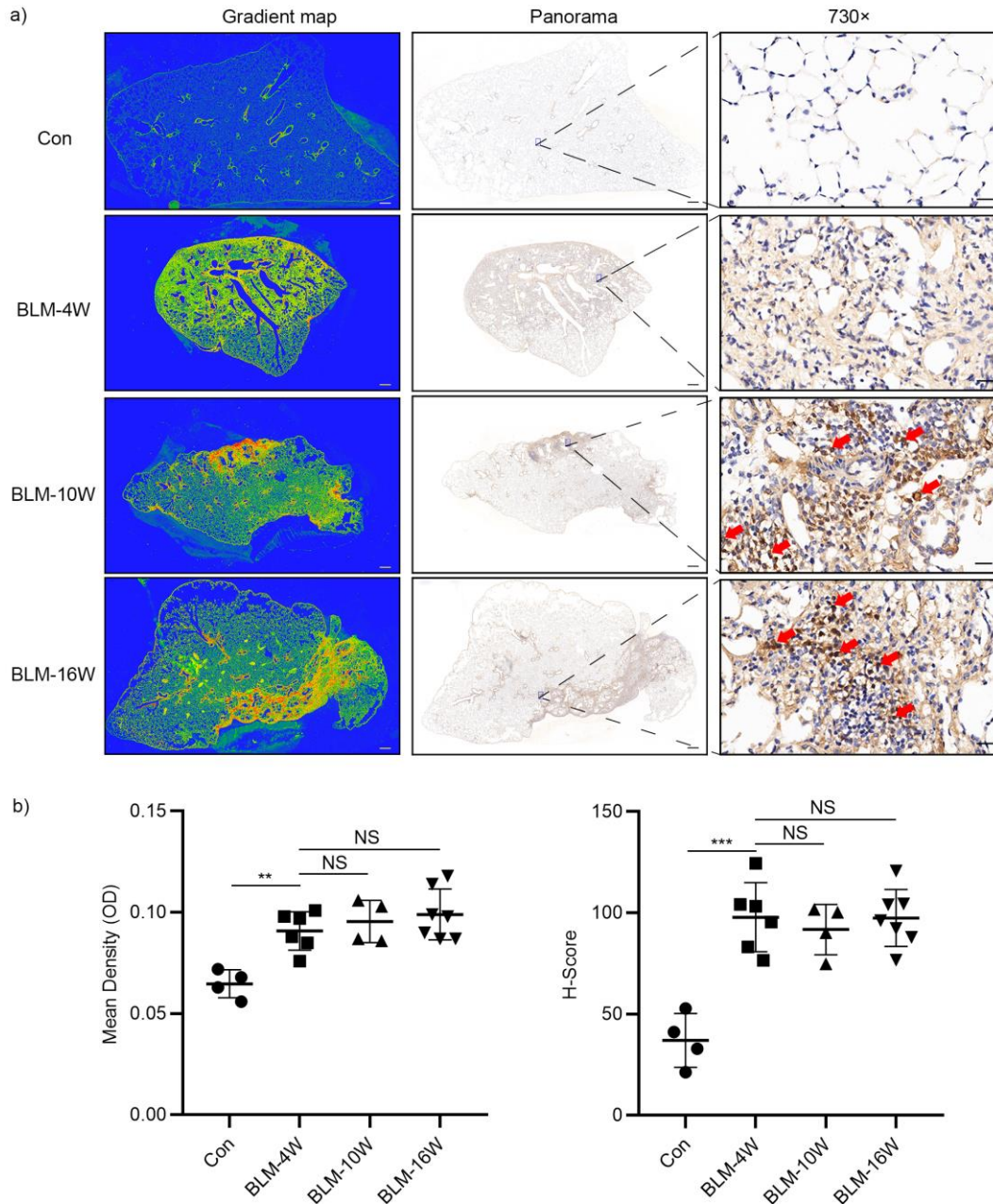


**Figure 7. Immunohistochemical analysis of hydroxyproline content.** a) Immunohistochemical stained panorama images (*middle*) for hydroxyproline and their respective gradient maps (*left*) of the indicated lung tissues. Scale bar = 500  $\mu\text{m}$ . The right column indicates high power field of positive staining areas (Scale bar = 20  $\mu\text{m}$ ). Arrows show cells with extremely strong intracellular immunostaining of hydroxyproline. The mean intensity of immunostaining signals as well as the H-Score for hydroxyproline were calculated. Data are expressed as mean  $\pm$  SD, n = 4-6.

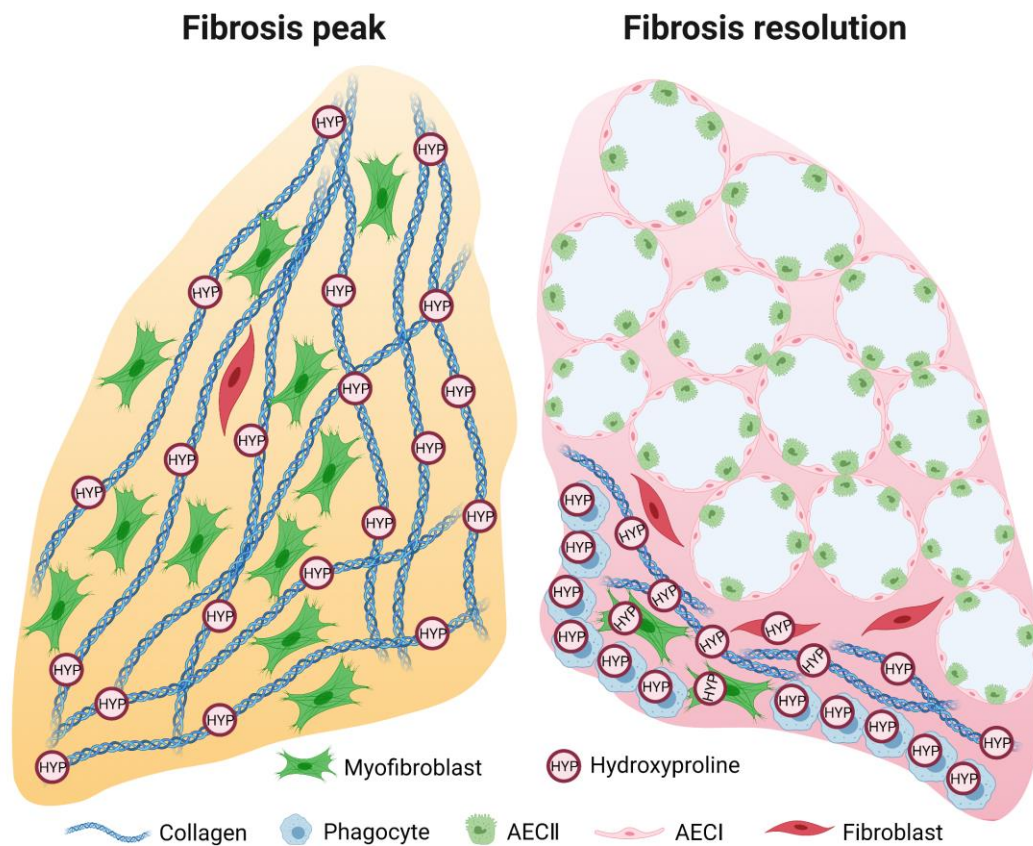


**Figure 8. Schematic hypothesis of constant contents of hydroxyproline from fibrosis peak to valley periods.** At the phase of lung fibrosis peak, native collagens that contain rich hydroxyproline were largely deposited within the lung interstitium. Upon the resolution of bleomycin-induced pulmonary fibrosis, collagen fibers might undergo enzymatic digestion and then were localized within a narrowed area or even absorbed into the intracellular compartment. However, these hydroxyproline-containing substances could not be completely removed and catabolized, leading to the constant contents of total hydroxyproline.

# **Intracellular Hydroxyproline Imprinting Following Resolution of Bleomycin-Induced Pulmonary Fibrosis**

## **Online supplementary material**

### **Methods**

#### *Animals and treatments*

Male C57BL/6J mice (6-8 weeks) were provided by Hunan SJA Laboratory Animal Co., Ltd (Changsha, Hunan, China), and housed in cages with an ad libitum access to water and food at a room maintained at 25°C. Bleomycin (Hisun Pfizer Pharmaceuticals Co., Ltd., Hangzhou, China) was dissolved in sterile 0.9% saline and administrated as a single dose of 2.0 mg/kg per animal. Control animals received equal volumes of saline alone. All animals received intratracheal instillation (IT) of either bleomycin or saline on day 0 as previously described [1, 2]. Mice were randomly assigned to seven weight-matched experimental groups: (1) IT bleomycin, week 1; (2) IT bleomycin, week 2; (3) IT bleomycin, week 3; (4) IT bleomycin, week 4; (5) IT bleomycin, week 10; (6) IT bleomycin, week 16; and (7) IT saline. In order to describe the time-course of bleomycin-induced lung fibrosis, the mice in group (6) were captured continuous dynamic CT images before bleomycin instillation and on weeks 1, 2, 3, 4, 7, 10, 12, and 16 following IT bleomycin using micro-computed tomography (micro-CT) analysis (PINGSENG Healthcare Inc., SNC-100, China). On weeks 1, 2, 3, 4, 10, and 16 following IT bleomycin or saline instillation, animals were anesthetized with 1% sodium pentobarbital (50 mg/kg body weight).

#### *In vivo micro-CT analysis*

Mice were anesthetized by isoflurane and transferred into an apparatus to scan the lungs. High-resolution scans (50 µm voxel size) were acquired using the Super Nova CT (PINGSENG Healthcare Inc., SNC-100, Kunshan, Jiangsu, China) according to the manufacturer's instructions and analyzed with the algorithms of three-dimensional (3D) finite element (AVATAR 1.5.0, PINGSENG Healthcare Inc., China). Briefly,

axial and coronal images were analyzed for identical *in vivo* signs (e.g., right bronchus bifurcation), which were defined as fibrotic areas. 3D Slicer (<http://www.slicer.org>.) is a free open-source extensible software applied for medical image computing and visualization [3]. The CT cross section of the lungs is set as a threshold to include only those voxels that mainly contain air, converting these binary images into 3D volume for visualization and quantification of aerated lung volume [4]. Briefly, two-dimensional regions of interest were identified by thresholding according to lung CT HU in the body. The steps are including: 1) select volume of interest, 2) mask and threshold volume of lung, 3) subtract and extract masked volume from original volume, 4) manually subtract the airway and edge components. Manual contouring techniques and body marks can be used to further enhance the segmentation of 3D reconstruction and calculate the lung volume.

#### *CT volumetry*

We used a semi-automatic lung segmentation algorithm with 3D slicer, which was divided into four categories by CT attenuation density. The hilar structures of the lungs, trachea, and main bronchi were eliminated manually as needed. Lung regions were classified into 4 categories by CT attenuation densities: 1) hyper-inflated, density between  $-1000$  and  $-861$  Hounsfield units (HU); 2) normally-aerated, density between  $-860$  and  $-435$  HU; 3) poorly-aerated, density between  $-434$  and  $-121$  HU; and 4) non-aerated, density between  $-120$  and  $+121$  HU [5]. Density attenuation classification on micro-CT lung is challenging because the density of  $-120$  to  $+121$  HU has a great similarity with the surrounding soft tissue, especially the fibrotic lung tissue area. Briefly, the segmentation process is as follows: a total mask was established to cover the density range of  $-1000$  to  $+121$  HU. 8-10 axial CT images that could be recognized in the lung were painted, and the slices were filled between slices to cover the entire lung. Some unnecessary areas of the entire lung were eliminated carefully. After the lung mask is formed, the density attenuation is distinguished according to different classification criteria mentioned above.

### *H&E and Sirius red staining*

Left lungs were instilled with 4% paraformaldehyde, fixed in this stationary liquid overnight at room temperature, and embedded in paraffin blocks. Then, lung sections (3 µm) were prepared, deparaffinized and stained with hematoxylin and eosin (H&E) or sirius red staining according to the manufacturer's instructions.

### *Automated histological image analysis*

The whole slide images (WSI) of H&E or sirius red stained lung sections were acquired by the Aperio CS2 whole slides scanner (Leica, Germany) for analysis. Scans were accomplished by the fully automated mode and 20× objective. These digital images were then converted to panoramic images by Aperio Image Scope (Version 12.3.2.5030, Leica Biosystems). Automated WSI analysis were performed using an Orbit Image Analysis software (Actelion Pharmaceuticals Ltd, Allschwil, Switzerland) as described previously [6, 7].

### *Immunohistochemistry*

Lung tissue sections (3 µm) were dewaxed and rehydrated using graded alcohol, followed by antigen retrieval with high pressure cooking for 2 min in 0.01 M sodium citrate buffer solution (pH 6.0). The endogenous peroxidase activity was eliminated using 3% H<sub>2</sub>O<sub>2</sub> in methanol for 10 min. After incubation with 5% BSA for 1 h, the sections were stained with rabbit anti-hydroxyproline antibody (#73812, Cell Signaling Technology, USA) or rabbit IgG overnight at 4°C at a dilution of 1:100, and then incubated with strept avidin-biotin complex (ABC) immuno detects kit (BOSTER, China) for 30 min at room temperature. All sections were subjected to color development with peroxidase-conjugated avidin/biotin and 3'-3-diaminobenzidine (DAB) substrate (Beyotime Biotechnology) and counterstaining with haematoxylin.

### Immunohistochemical staining image analysis

DAB-stained lung slides were scanned using a 3D Scan Panoramic Histech scanner (3D Histech Kft. Budapest, Hungary) at 40× objective magnification and Aperio ScanScope CS2 (Aperio Technologies, USA) at 40× objective magnification. The Positive Pixel Count v9 algorithm preload in Aperio ScanScope CS2 software was used for hydroxyproline immunochemistry analysis. The gradient map was analyzed by CaseViewer (3D Histech Kft. Budapest, Hungary). The Mean Density of immunostaining signals as well as the H-Score for hydroxyproline were calculated according to the method described as previously [8].

### *Hydroxyproline levels*

The hydroxyproline levels in the lungs were examined using a commercial kit (Nanjing Jiancheng Bioengineering Institute, Nanjing, China) according to the manufacturer's instructions.

### *RNA extraction and quantitative real-time PCR (qPCR)*

Total RNA (1 µg) was reverse transcribed using PrimeScript™ Reverse Transcriptase (Takara, Kyoto, Japan) and quantitative real-time PCR was performed using SYBR qPCR premix (Takara). The specific sequences of forward (F) and reverse (R) primers used are as follows (5'-3'): AACGAGATCGAGCTCAGAGG (F) and GACTGTCTTGCCCCAAGTTC (R) for mouse Collagen 1, GCGACGGTATTCTGTAAAGTGG (F) and GGACAGGGCTTTGGCAGTT (R) for mouse Fibronectin, and AGTGGCAAAGTGGAGATT (F) and GTGGAGTCATACTGGAACA (R) for mouse GAPDH. Relative levels of mRNA expression were normalized to GAPDH expression for each gene.

### *Collagen hybridizing peptide (CHP) staining*

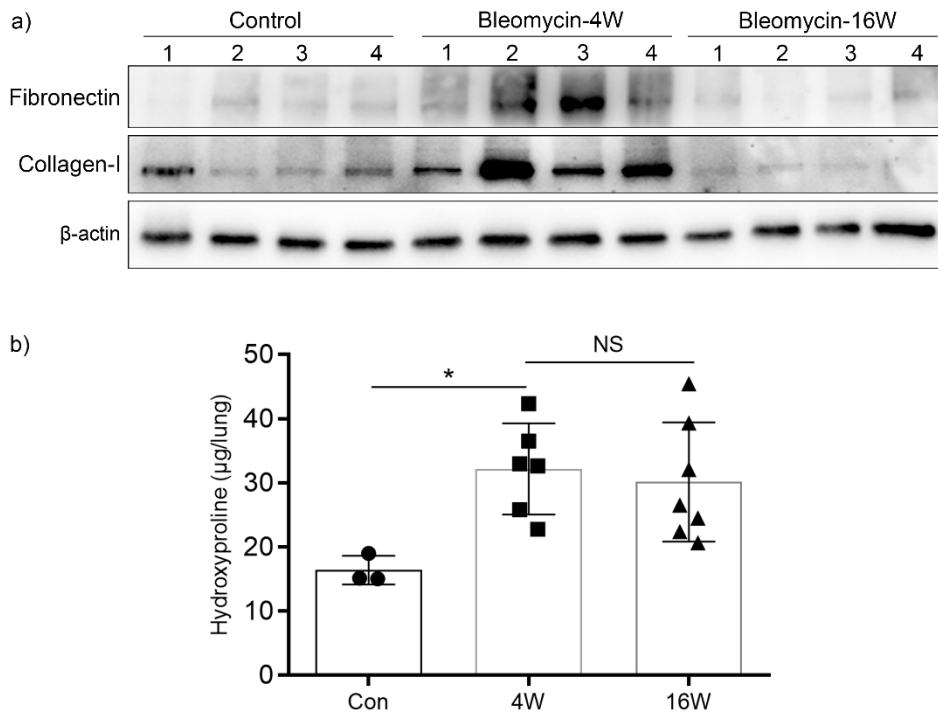
The collagen hybridizing peptide (CHP) staining kit used in this experiment was purchased from 3Helix Inc. Normal mice and pulmonary fibrosis paraffin embedded sections after week 1, 2, 3, 4, 16 were prepared for CHP staining. For Paraffin embedded lung tissue sections, lung tissue sections were washed with xylene (3 times, 10min/ time), 100% ethanol (2 times, 5min/time), 95% ethanol (3min), 85% ethanol (3min), 75% ethanol (3min), 50% ethanol (3min) and PBS (3 times, 5min/time). The deparaffinized tissue was directly used for staining without any antigen-retrieval process. After the embedding material was removed, 5% goat serum in PBS was added to the tissue sections and incubated for 20 min at room temperature to block nonspecific binding. Since Cy5-CHP [ $\text{scy5-(GPO)}_9$ ] will self-assemble into homotrimer in solution over time (for example, during storage at 4 ° C) and lose the driving force of its collagen hybridization, the trimer CHP was pyrolyzed to single chain at 80 ° C (10min) before using. In order to prevent unnecessary thermal denaturation of the tissue, the CHP solution which was heating to 80 ° C was rapidly quenched to room temperature (< 2min) immediately before adding to the tissue sample. Tissue samples were incubated overnight in a humidity chamber at 4 ° C (15  $\mu$  M, Cy5-CHP, 200  $\mu$  L for each piece of tissue). After staining, the slides were incubated at room temperature in 100 mL PBS for 5min, free substances were removed, washed repeatedly for 3 times, and sealed with anti-fluorescence quencher. EVOS fluorescence microscope imaging was finally performed.

### *Western Blot*

Lung tissues were extracted using RIPA lysis buffer with protease inhibitor cocktail (Sigma-Aldrich, USA) and then centrifuged (12000 rpm, 15 min, 4°C) to obtain supernatants. The total protein concentration was measured by bicinchoninic acid (BCA). Protein was separated by 10% SDS-PAGE and electrotransferred to PVDF-membranes (Millipore, Bedford, MA). The immunoblots were probed with appropriate primary antibodies overnight at 4°C, followed by incubation with the

corresponding secondary antibodies. The blots were visualized with ECL-Plus reagent (Yeasen Biotech Co., Ltd., Shanghai, China). The results were analyzed by a densitometry system named Image J. The antibodies used in this study include: anti-collagen 1 (Cat# 67288-1-Ig), anti-fibronectin (Cat# 15613-1-AP) and anti- $\beta$ -actin (Cat# 66009-1-Ig) polyclonal antibodies were purchased from Proteintech (Wuhan, Hebei, China). The HRP-labeled Goat Anti-Rabbit/Mouse IgG (H + L) were purchased from Abcam Biotechnology (Cambridge, MA, USA).

**Supplementary figure.** Time course of ECM levels and hydroxyproline content.



**Supplementary figure.** a) Western blot was used to determine the protein levels of Collagen- I and fibronectin in the lungs of bleomycin and saline-treated mice, at different points. b) Hydroxyproline levels in the lungs of bleomycin and saline-treated mice, at different points. Data are expressed as mean  $\pm$  SD, n = 6, \*\*\*  $p < 0.001$ .

## References:

1. Kremer S, Breuer R, Lossos IS, et al. Effect of immunomodulators on bleomycin-induced lung injury. *RESPIRATION* 1999; 66(5): 455-462.
2. Laxer U, Lossos IS, Gillis S, et al. The effect of enoxaparin on bleomycin-induced lung injury in mice. *EXP LUNG RES* 1999; 25(6): 531-541.
3. Fedorov A, Beichel R, Kalpathy-Cramer J, et al. 3D Slicer as an image computing platform for the Quantitative Imaging Network. *MAGN RESON IMAGING* 2012; 30(9): 1323-1341.
4. Ashton JR, West JL, Badea CT. In vivo small animal micro-CT using nanoparticle contrast agents. *FRONT PHARMACOL* 2015; 6: 256.
5. Mecozzi L, Mambrini M, Ruscitti F, et al. In-vivo lung fibrosis staging in a bleomycin-mouse model: a new micro-CT guided densitometric approach. *Sci Rep* 2020; 10(1): 18735.
6. Stritt M, Stalder AK, Vezzali E. Orbit Image Analysis: An open-source whole slide image analysis tool. *PLOS COMPUT BIOL* 2020; 16(2): e1007313.
7. Seger S, Stritt M, Vezzali E, et al. A fully automated image analysis method to quantify lung fibrosis in the bleomycin-induced rat model. *PLOS ONE* 2018; 13(3): e193057.
8. Paschalis A, Sheehan B, Riisnaes R, et al. Prostate-specific Membrane Antigen Heterogeneity and DNA Repair Defects in Prostate Cancer. *EUR UROL* 2019; 76(4): 469-478.